3542 *Chem. Mater.* **2009,** *21,* 3542–3548
DOI:10.1021/cm900132j

CHEMISTRY OF MATERIALS
Article

Metallization of Silicon Nanowires and SERS Response from a Single Metallized Nanowire

Cheng Fang,*[,†] Ajay Agarwal,[†] Effendi Widjaja,[‡] Marc V Garland,[‡] She Mein Wong,[†] Linn Linn,[†] Nizamudin Mohamed Khalid,[‡] Shaik Mohamed Salim,[‡] and Narayanan Balasubramanian[†]

[†]*Institute of Microelectronics, A*STAR (Agency for Science, Technology and Research), 11 Science Park Road, Singapore Science Park II, Singapore, and* [‡]*Institute of Chemical and Engineering Sciences, A*STAR (Agency for Science, Technology and Research), 1 Pesek Road, Jurong Island, Singapore*

Received January 15, 2009. Revised Manuscript Received June 2, 2009

A simple method was demonstrated to metallize silicon (Si) nanowire (NW) just by dipping it into an aqueous deposition solution for several minutes. During the metallization process, metal ions were reduced and deposited on the top of the Si NW (where surface Si was oxidized). The surface silicon oxide was simultaneously dissolved and removed by hydrogen fluoride (HF), so that the deposition reaction was sustainable and controllable. The deposited silver (Ag) nanoparticles (NPs) uniformly self-assembled along the Si NW and developed into a metal covering with the NW as its core. Not only Ag^{+} but also Cu^{2+}, Pd^{2+}, Co^{2+}, Au^{3+}, and Pt^{4+} were deposited to metallize the Si NW using the simplified metallization process. Applications of the new nanocomposite materials were also explored. When the resulting Ag NP/Si NW was tested as a surface-enhanced raman scattering (SERS) substrate, an extremely strong signal was observed and a detection limit of ~600 molecules or 200−300 Ag NPs per laser spot was reached. The significantly enhanced SERS effect appears to be associated with the close packing of the neighboring NPs that self-assemble along the highly curved NW.

1. Introduction

Interest in semiconductor nanowire (NW) has accelerated recently due to its wide-range of amazing properties.[1−3] Research concerning its surface chemistry,[4,5] conductivity,[6] and optical properties[7−9] has been carried out, and its application as a sensor, microcircuit, or building block for other nanodevices has been investigated. Metallized NW, which is a nanocomposite material, has also attracted considerable attention because it can be used as a battery electrode, solar cell material, catalyst, nanophotonic, SERS (surface-enhanced raman scattering) substrate, etc.[8−11] However, the current metallization methods of silicon (Si) NW, such as vapor vacuum implantation[12] and argon-ion sputtering,[13] are complicated or the nanoparticles (NPs) grow inhomogeneously and are distributed non uniformly.[8,9] In this report, a facile method is demonstrated to metallize a Si NW array just by dipping it into a deposition solution. On the other hand, the metal deposition on the Si surface, which includes nucleation and subsequent growth, is still not well understood because there are numerous factors affecting the deposition process.[14−18] However, because of the redox displacement reaction used, the metal deposition in the present report can be focused onto a small area of the exposed Si NW surface, thereby simplifying the process and making it more controllable. Herein, the Si NW is employed simultaneously as a deposition template and a reducing agent. By using this metallization method, several new nanocomposite materials are fabricated and their applications are studied. The metallized

*To whom correspondence should be addressed. Phone: 65 6770 5754. Fax: 65 6773 1914. E-mail: fangc@ime.a-star.edu.sg.

(1) Cui, Y.; Wei, Q. Q.; Park, H.; Lieber, C. M. *Science* **2001**, *293*, 1289–1292.
(2) Patolsky, F.; Zheng, G. F.; Lieber, C. M. *Anal. Chem.* **2006**, *78*, 4261–4269.
(3) Fang, C.; Föll, H.; Carstensen, J. *Nano Lett.* **2006**, *6*, 1578–1580.
(4) Sun, X. H.; Peng, H. Y.; Tang, Y. H.; Wong, W. S.; Lee, C. S.; Lee, S.-T. *J. Appl. Phys.* **2001**, *89*, 6396–6399.
(5) Ma, D. D. D.; Lee, C. S.; Au, F. C. K.; Tong, S. Y.; Lee, S.-T. *Science* **2003**, *299*, 1874–1877.
(6) Fujii, H.; Kanemaru, S.; Matsukawa, T.; Itoh, J. *Appl. Phys. Lett.* **1999**, *75*, 3986–3988.
(7) Chen, Y.; Peng, B.; Wang, B. *J. Phys. Chem. C* **2007**, *111*, 5855–5858.
(8) Leng, W.; Yasseri, A. A.; Sharma, S.; Li, Z.; Woo, H. Y.; Vak, D.; Bazan, G. C.; Kelley, A. M. *Anal. Chem.* **2006**, *78*, 6279–6282.
(9) Yasseri, A. A.; Sharma, S.; Kamins, T. I.; Li, Z.; Williams, R. S. *Appl. Phys. A: Mater. Sci. Process.* **2006**, *82*, 659–664.
(10) Li, J.; Tang, S.; Lu, L.; Zeng, H. C. *J. Am. Chem. Soc.* **2007**, *129*, 9401–9409.
(11) Hu, H.; Shao, M.; Zhang, W.; Lu, L.; Wang, H.; Wang, S. *J. Phys. Chem. C* **2007**, *111*, 3467–3470.
(12) Li, C.-P.; Wang, N.; Wong, S. P.; Lee, C.-S.; Lee, S.-T. *Adv. Mater.* **2002**, *14*, 218–221.
(13) Li, C.-P.; Sun, X. H.; Wong, N. B.; Lee, C.-S.; Lee, S.-T.; Teo, B. K. *J. Phys. Chem. B* **2002**, *106*, 6980–6984.
(14) Leger, C.; Elezgaray, J.; Argoul, F. *Phys. Rev. E* **2000**, *61*, 5452.
(15) Oberholtzer, F.; Barkey, D.; Wu, Q. *Phys. Rev. E* **1998**, *57*, 6955.
(16) Wen, X.; Xie, Y.-T.; Mak, M. W. C.; Cheung, K. Y.; Li, X.-Y.; Renneberg, R.; Yang, S. *Langmuir* **2006**, *22*, 4836–4842.
(17) Fang, J.; You, H.; Kong, P.; Yi, Y.; Song, X.; Ding, B. *Cryst. Growth Des.* **2007**, *7*, 864–867.
(18) Pasquale, M. A.; Marchiano, S. L.; Schilardi, P. L.; Salvarezza, R. C.; Arvia, A. J. *Phys. Rev. E* **2002**, *65*, 041608.

Published on Web 07/20/2009

NW with a uniform distribution of silver (Ag) NPs is tested as a SERS substrate and a high enhancement is observed even from a single metallized NW alone.

Since its discovery in 1977, SERS has received more and more attention from researchers around the world.[19−21] Its high sensitivity, which originates from the enhancement on the substrate surface, provides the potential for becoming a new tool for single molecule detection.[22,23] The commonly used SERS substrates include electrochemically roughened metal surfaces, metal NP arrays, nanofabricated substrates, etc.[20,24] With regard to the roughened metal surfaces or the NP arrays, although a high enhancement efficiency has been achieved, the distribution of so-called hot-spots (the positions where maximum enhancements occur) is random because of the difficulty in controlling the structures on a nanoscale. However, controllable nanostructures are crucial for SERS because the strong electromagnetic field on the metal surface, which is the main contributor to Raman enhancement, exponentially decreases with a characteristic length scale of ~2 nm.[20] Numerous technologies have been developed in an attempt to control the substrate's structure on the nanoscale in the hope to obtain a more uniform distribution of nanostructures.[24,25]

To bring SERS a step closer to practical application, it is advantageous to prepare the SERS substrate at the point of use because a fresh and oxide-free surface can yield a higher enhancement and simplify the sample preparation process. Because the commonly used metal for SERS substrates is Ag and Ag^+ is easily reduced, it is possible to deposit Ag NP in a straightforward manner onto a template surface at the point of use.[26] Moreover, Si is a known reducing agent in the presence of metal ions and can be used as the deposition template.[27] However, the random distribution and aggregation of the deposited NPs, and the appearance of dendrites on flat Si surfaces can result in a nonuniform SERS substrate and a low reproducible Raman signal.[27,28] A similar phenomenon is observed on porous Si surfaces even though the porous structure can increase the reaction area.[29,30] Alternatively, Si NW can be used as a template for the SERS substrate because it also exhibits a high specific surface area for the deposition reaction.[27] The resulting Ag NPs that are deposited onto the small and high curved NW surface can be expected to exhibit considerably different properties. To achieve a sustainable and controllable deposition reaction, hydrogen fluoride (HF) is introduced into the deposition solution to remove the silicon oxide surface layer on the top of Si NW. Such an oxide layer maybe disrupts the continuous deposition reaction.[31,32]

The arrangement of the NWs also influences the final quality of the SERS substrate. For example, upon contacting an Ag^+ solution, a random arrangement of Si NWs can be expected to result in a nonuniform formation of Ag NPs on the Si surfaces. If two NWs lie closely, perhaps the deposition reaction occurring on one NW can interfere with that occurring on another one because of the overlapping diffusion layer of reactants or products. In contrast, a well-ordered array of Si NW can be expected to result in a much more uniform deposition of Ag NPs. As for a regular arrangement of straight NW with a controllable separating distance, each part of NW is the same as the rest so that every NW can experience the similar deposition reaction environment. As a consequence, the metallization can homogeneously occur on every part of NW and a uniform distribution of SERS substrate is obtained in turn. Moreover, the actual Raman measurements will also be influenced. A small laser spot-size (diameter of $1-1.5\,\mu$m) on a random array may focus on one or even more than one NW simultaneously, whereas a small laser spot-size focused on a regular array of NWs should be more reproducible.[8,9]

In this report, the metallization process of a Si NW array using a simple liquid-phase deposition solution is reported. Subsequently, the self-assembled nanocomposite Ag NP/Si NW is tested as a SERS substrate.

2. Experimental Section

With the exception of ammonium fluoride etchant (Merck, TB 1063), all chemicals were purchased from Sigma-Aldrich. Si NW arrays (chips) were fabricated at IME (Institute of Microelectronics), A*STAR, Singapore.[33] A schematic drawing of the Si NW chip (NW and conductive circuit) is shown in Figure 1a. The relatively thin surface layer of native oxide on the Si NW (*n*-type) was effectively removed by dipping the array into Ammonium Fluoride Etchant for 10−30 s, whereas the thick layers of silicon oxide on the Si wafer bed and the silicon nitride on the conductive circuit were not significantly etched or dissolved. Metallization of the exposed NW was immediately performed by dipping it into a fresh deposition solution for various deposition times with gentle shaking in the dark. Transmission electron microscopy (TEM, Philip, with PW6061/25 EDX) and scanning electron microscopy (SEM, JSM-6700F, Japan) were employed for physical characterization of the metallized NW. Regarding the peeling-off of the resulting metal covering from

(19) Kneipp, K.; Kneipp, H.; Itzkan, I.; Dasari, R. R.; Feld, M. S. *Chem. Rev.* **1999**, *99*, 2957–2975.
(20) Haynes, C. L.; McFarland, A. D.; Duyne, R. P. V. *Anal. Chem.* **2005**, *77*, 338A–346A.
(21) Vandenabeele, P.; Edwards, H. G. M.; Moens, L. *Chem. Rev.* **2007**, *107*, 675–686.
(22) Nie, S.; Emory, S. R. *Science* **1997**, *275*, 1102–1106.
(23) Sasic, S.; Itoh, T.; Ozaki, Y. *J. Raman Spectrosc.* **2005**, *36*, 593–599.
(24) Fang, C.; Agarwal, A.; Buddharaju, K. D.; Khalid, N. M.; Salim, S. M.; Widjaja, E.; Garland, M. V.; Balasubramanian, N.; Kwong, D.-L. *Biosens. Bioelectron.* **2008**, *24*, 216–221.
(25) Domke, K. F; Zhang, D.; Pettinger, B. *J. Am. Chem. Soc.* **2007**, *129*, 6708–6709.
(26) Hyning, D. L. V.; Klemperer, W. G.; Zukoski, C. F. *Langmuir* **2001**, *17*, 3128–3135.
(27) Peng, K.; Hu, J.; Yan, Y.; Wu, Y.; Fang, H.; Xu, Y.; Lee, S.; Zhu, J. *Adv. Funct. Mater.* **2006**, *16*, 387–394.
(28) Zhang, Y.; Ang, S. S.; Tay, A. A. O. *Langmuir* **2003**, *19*, 6802–6806.
(29) Chan, S.; Kwon, S.; Koo, T.-W.; Lee, L. P.; Berlin, A. A. *Adv. Mater.* **2003**, *15*, 1595–1598.
(30) Lin, H.; Mock, J.; Smith, D.; Gao, T.; Sailor, M. J. *J. Phys. Chem. B* **2004**, *108*, 11654–11659.
(31) Zhang, P.; Zhou, X.; Tang, Y.; Sham, T. S. *Langmuir* **2005**, *21*, 8502–8508.
(32) Kalkan, A. K.; Fonash, S. J. *J. Phys. Chem. B* **2005**, *109*, 20779–20785.
(33) Gao, Z.; Agarwal, A.; Trigg, A. D.; Singh, N.; Fang, C.; Tung, C.-H.; Fan, Y.; Buddharaju, K. D.; Kong, J. *Anal. Chem.* **2007**, *79*, 3291–3297.

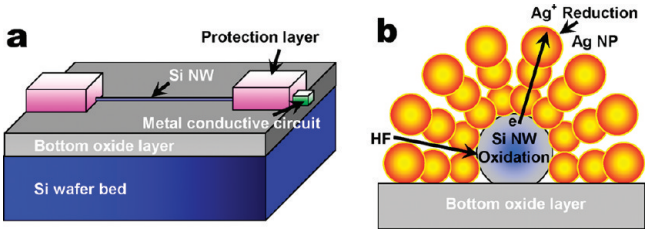

Figure 1. Schematic drawing of (a) the Si NW chip and (b) the cross-section view of Ag NPs assembled along the Si NW. For clarity of presentation, the metal conductive circuit is drawn partly exposed in (a). The redox metallization process is presented in (b).

the Si NW and the lifting-off of the nanocomposite materials from the bottom oxide layer, the metallized Si NW was dipping into a solution of 1 M HF for 1−5 min.

As for the SERS measurements, two methods were used to load the Raman scatterer Rhodamine 6G (R6G) onto the metallized NW array. In the first case, the NW array was incubated in an aqueous solution of ~5 mL containing 1×10^{-7} M R6G or other concentrations for 3 h in the presence of 1 mM NaCl. It was then washed with deionized water and dried with nitrogen, and the Raman signal was collected. In the second case, ~0.2 μL of 1×10^{-7} M R6G aqueous solution was dropped onto the freshly metallized NW array. After the solution was dried, the Raman signal was collected directly.

All SERS spectra were recorded in the air using a Renishaw In Via Reflex Raman Microscope (Renishaw plc., UK) equipped with a 300 mW near-infrared 785 nm diode laser. The laser beam was focused into a spot on the substrate with a diameter of 1.0−1.5 μm through an objective lens (50×) (Leica Imaging Microscope) with a lateral spatial resolution of 1 μm. Stokes Raman scattering were collected in a wavenumber range of 600−2000 cm^{-1} with a resolution of ~1.0 cm^{-1} for an exposure time of 10 s for each measurement. For image mapping, the Raman spectra were collected from a set of grid points (1 μm separation). The intensity map was generated using the integrated signal of the peak at 1510 cm^{-1} after removing background.

3. Results and Discussion

3.1. Ag Deposition. The Si NW was utilized as the deposition template and its schematic drawing is presented in Figure 1a. The original design of the chip is for a complete biosensor but only the exposed NW array is the area of interest in this report. The metallization process is a redox reaction, which includes the reduction of metal ions to be deposited as NPs and the oxidation of Si to provide the needed electrons. A cross-sectional view of a metallized NW and the redox displacement reaction are presented in Figure 1b. There is neither extra polarization potential nor net current so that it is also an electroless reaction. In the presence of HF in the deposition solution, the Si NW surface is hydrogen-terminated. Upon reduction of Ag^+, silicon oxide is momentarily reformed but quickly removed again by HF to yield a sustainable metallization process.[27,34]

Upon exposure of the Si NW to the deposition solution (HF + $AgNO_3$), the nucleation process begins, as observed in Figure 2. However, all nuclei were apparently not created immediately but instead progressively within the first 30 s (Figure 2a−d), suggesting not an instantaneous but a progressive nucleation process.[26,35,36] In the end, the NW surface becomes fully covered with Ag NPs, as shown by the rather complete surface saturation with Ag NPs (images d and e in Figure 2).

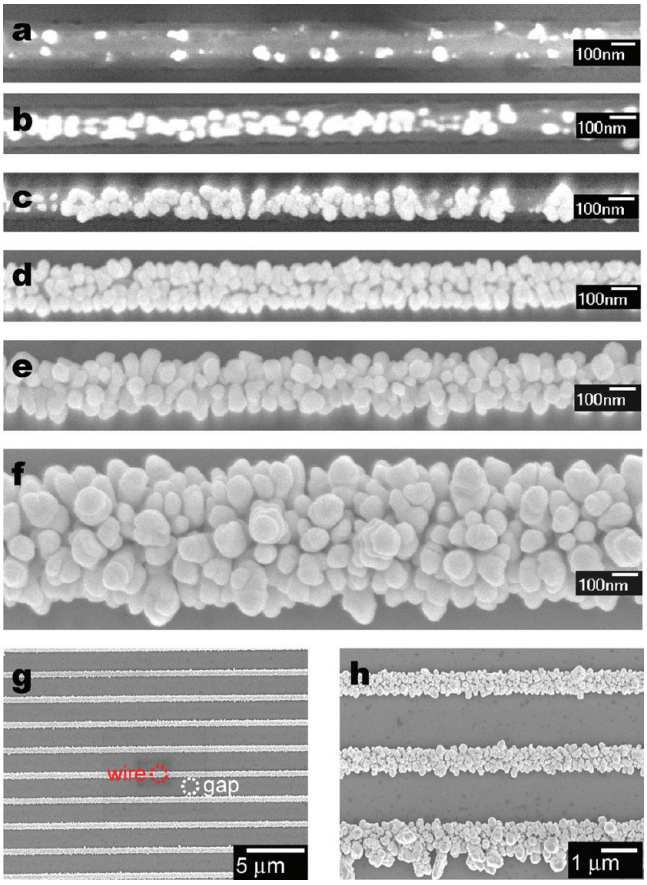

Figure 2. SEM pictures of the metallized NW after different deposition time. The metallization was conducted in 1×10^{-3} M HF + 1×10^{-4} M $AgNO_3$ for (a) 1 s, (b) 5 s, (c) 10 s, (d) 30 s, (e) 1 min, and (f−h) 5 min, respectively. (g) Interior part of the NW array, and (h) peripheral part of the NW array. The bottom metallized NW in (h) is the edge one in the NW array. The dashed-line circles in (g) indicate the laser spot's position for the SERS spectra shown in Figure 6c.

It has been reported that the saturation coverage of Ag NP on a hydrogen-terminated Si (100) surface is ~2×10^9 cm^{-2} when an electrochemical potential pulse was employed.[37] The estimated value from Figure 2d, however, is ~1.7×10^{11} cm^{-2}. There are several possible reasons for the difference. (i) The NW template has not only an extremely high specific surface area but its geometry (a thin wire exposed to the deposition solution in all directions except the bottom, as shown in Figure 1b) also improves the transport efficiency of the reactant ions for nucleation.;[32] (ii) HF can etch and refresh the Si surface continuously, which provides an opportunity

(34) Harraz, F. A.; Tsuboi, T.; Sasano, J.; Sakka, T.; Ogata, Y. H. *J. Electrochem. Soc.* **2002**, *149*(9), C456–C463.
(35) Simm, A. O.; Ji, X.; Banks, C. E.; Hyde, M .E.; Compton, R. G. *ChemPhysChem* **2006**, *7*, 704–709.
(36) Oskam, G.; Long, J. G.; Natarajan, A.; Searson, P. C. *J. Phys. D: Appl. Phys.* **1998**, *31*, 1927–1949.
(37) Stiger, R. M.; Gorer, S.; Craft, B.; Penner, R. M. *Langmuir* **1999**, *15*, 790–798.

for the nucleation to regenerate, although the decease in some nuclei should also be taken into account.[9] (iii) The polycrystalline Si NW was used in this report so that the number of the crystal defects was much more than that on the single-crystal Si surface. The nucleation density is likely related to the surface defect density.[37] (iv) An electroless deposition was employed in this report and a slow nucleation process was observed in turn. In Figure 2d, the electroless reaction takes ~30 s to reach saturation coverage, whereas it takes only 20 ms when an electrochemical pulse is applied. For a progressive nucleation process, a high coverage is acceptable after a long nucleation period.[37] On the other hand, perhaps the observable nuclei in Figure 2d are generated not only on the NW surface but also on the Ag NP surface, as presented in Figure 1b. It should be noted that the concentration of HF or Ag^+ has been optimized, as shown in Figures S1 and S2 in the Supporting Information. That is, even the concentration can also affect the nucleation process.

The specific property of the metal ion also plays an important role on the nucleation. For example, the redox potential of each selected metal ion (see Table S1 in the Supporting Information) differs from that of Si and the difference provides the driving force for the deposition reaction.[34,36] The self-driving metallization process is initialized with the nucleation process, which is usually involved with either the overpotential or under-potential deposition.[12,38] As a consequence, the parameter mismatch of the atomic lattice between the deposited metal and the Si (see Table S2 in the Supporting Information) is critical for the formation of the first atomic layer of metal on the Si surface.[12] Moreover, the coordination interaction between the fluoride ion and the metal ions is capable of shifting the redox potential and the driving force, as discussed in the Supporting Information. Therefore, the different metal ions selected can lead to different morphology of the resulting covering, as shown in Figures S3−S5 of the Supporting Information.[9] The end product of the metallization process, however, originates not only from the nucleation process but also from its subsequent growth process.[26]

Similar to the nucleation, the growth process of an individual NP is also multifaceted[16,17,39] Although its mechanism is not yet completely understood, it is well-accepted that there are two growth processes, "coarsening" and "aggregation".[39] Coarsening means the growth of the larger particles at the expense of the smaller ones. Aggregation involves the growth of an individual particle from disoriented attachment to oriented attachment of the nanocrystal precursor. From Figure 2d to Figure 2f, almost a homogeneous growth of each NP is observed, suggesting that the coarsening is not dominant.

The regular arrangement of the NW array can hinder the inhomogeneous growth of NPs on the NW surface. That is because nearly every part of every NW is equivalent, at least in the interior part of the NW array. Unlike that on a flat surface, the deposition reaction is focused onto the mini surface area of the exposed NW. As a consequence, a uniform distribution of NPs along the Si NW core is observed in Figure 2f, g. In contrast, the peripheral part of NW array behaves differently. Perhaps it experiences more reactants or products than the interior part so that the NP growth gets faster on the peripheral part. This can lead to the appearance of "diffusion shielding" or overlapping diffusional zones.[37] Consequently, inhomogeneous nanostructures are obtained in Figure 2h. Even Ag nanolnukshuks are observed. Such structures have also been observed on a flat germanium surface.[40] Therefore, only the interior part of the metallizated NW array was studied and tested as the SERS substrate in the following discussion.

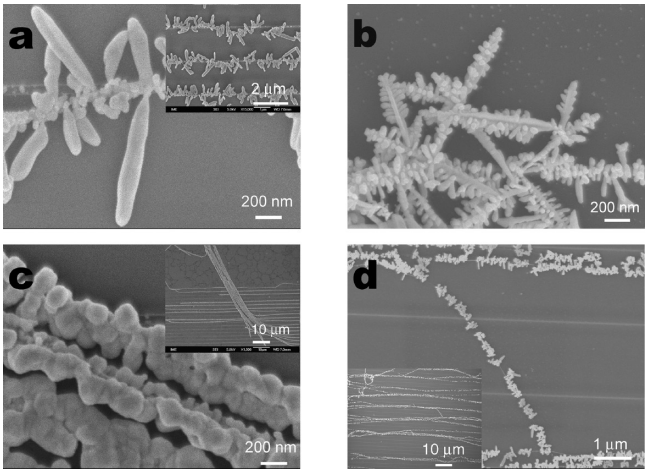

Figure 3. SEM pictures of (a, b) Ag nanosticks and (c, d) Ag NWs. The metallization was conducted in 1×10^{-2} M HF + 1×10^{-4} M $AgNO_3$ with vigorous shaking for (a, d) 10 or (b) 30 min, or in 1×10^{-3} M HF + 1×10^{-4} M $AgNO_3$ for (c) 30 min, respectively. After that, (c) the peeling-off of Ag covering from the Si NWs core or (d) the lifting-off of the metallized Si NWs from the bottom oxide layer was conducted by dipping the metallized NW array into 1 M HF for 1−5 min.

3.2. Morphology of the Ag Nanostructure. The obtained Ag nanostructures are shaped not only by the location of NW in the array but also by the deposition conditions, such as concentration, time, temperature, transport etc., as shown in Figure 3 and Figures S1 and S2 in the Supporting Information. There are two possible reasons for the appearance of nanosticks in Figure 3a: (i) the creation of a subsequent generation of nuclei on the NW has been suppressed and hence only nuclei growth occurs;[17,18,37] (ii) the growth of the NPs was faster along some particular crystallographic directions (nanostick) than along the rest.[41,42] In Figure 3b, the dendrite structures originate from the nanostick stem when the growth time has been prolonged.[16−18] The detailed discussion on the nucleation and growth process can be found in the Supporting Information.

(38) Sanchez, C.; Leiva, E. *J. Electroanal. Chem.* **1998**, *458*, 183–189.
(39) Penn, R. L.; Oskam, G.; Strathmann, T. J.; Searson, P. C.; Stone, A. T.; Veblen, D. R. *J. Phys. Chem. B* **2001**, *105*, 2177–2182.
(40) Aizawa, M.; Cooper, A. M.; Malac, M.; Buriak, J. M. *Nano Lett.* **2005**, *5*, 815–819.
(41) Fang, C.; Foca, E.; Xu, S.-F.; Carstensen, J.; Föell, H. *J. Electrochem. Soc.* **2007**, *154*, D45–D49.
(42) Lu, L.; Kobayashi, A.; Kikkawa, Y.; Tawa, K.; Ozaki, Y. *J. Phys. Chem. B* **2006**, *110*, 23234–23241.

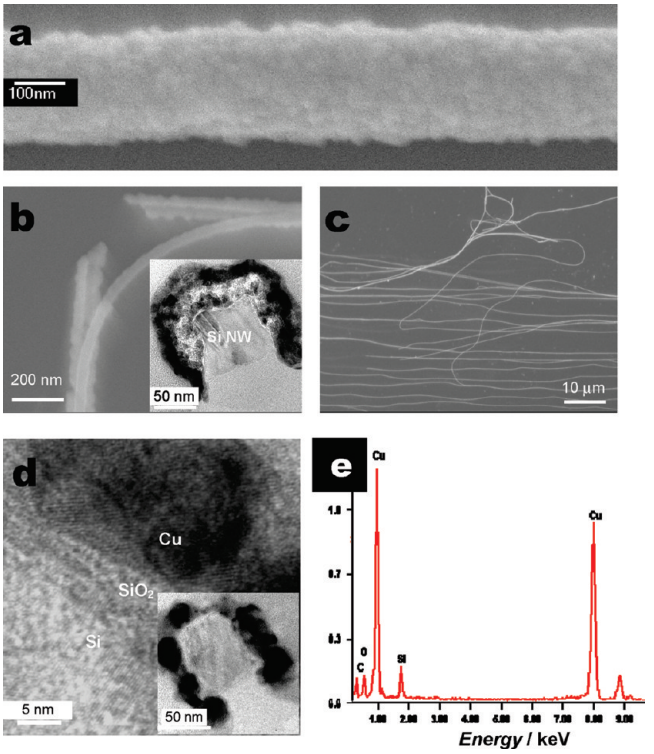

Figure 4. (a−c, top view) SEM, (b(inset) and d, all cross-section view) TEM pictures, and (e) EDX spectrum of the copper covering on Si NW. (b, c) Copper NWs can be seen after being peeled from the Si NW cores. The cross-section of the copper NW exhibits a semitubular shape in (b, d (inset)). The metallization was conducted in 1×10^{-3} M HF+1×10^{-4} M $Cu(NO_3)_2$ for 5 min except for 45 s in (d).

Exposure of the metallized NW array to a HF solution resulted in the peeling-off of the Ag coverings from their Si NW cores or the lifting-off of the nanocomposite materials from the bottom oxide layer. The Ag NWs with a semitubular shaped cross-section are obtained after being peeled off, as shown in Figure 3c. In contrast, Ag nanosticks attached to the Si NW cores do not easily fall off, as observed in Figures 3a−d. Perhaps the root of the Ag nanostick has grown further into a full-tubular shape to encircle or to anchor the free-standing Si NW core (Figure 3a) so that Ag "necklaces" were fabricated (Figure 3d). Another possible reason is that the etching of Si in the presence of HF can create pores in the bulk Si.[43] The metal deposition is capable of filling those pores and the formed nanosticks can extend into the deposition solution.[41] In other words, perhaps the Ag nanostick has roots that have grown into the porous Si, and it is therefore more difficult to detach.

3.3. Other Metals. As mentioned above, different metal ions can give rise to different nanostructures with different morphologies. Not only could Ag^+ be reduced and deposited onto the Si NW surface, but Cu^{2+} (Figure 4), Pd^{2+} (Figure 5), Co^{2+}, Au^{3+}, and Pt^{4+} (Figures S3−S5 in the Supporting Information) were also employed to metallize the Si NW in this report.

In the case of copper, a shiny covering was observable under an optical microscope. Such a shiny covering probably originates from a high density of nuclei on the NW surface.[36] The high density of nuclei can grow into a bulk covering, as shown in Figure 4a. The growth of copper was also faster than the other metals because of its high redox driving force (see Table S1 in the Supporting Information). It takes only 45 s (Figure 4d) to get an obvious covering on the NW surface with Cu, whereas other metals require 5 min or more (Figures S3−S5 in the Supporting Information).[28]

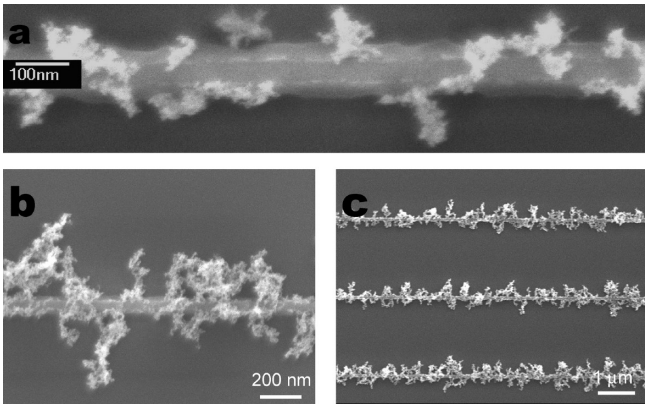

Figure 5. SEM pictures of the palladium network distributed along the Si NWs. The metallization was conducted in 1×10^{-3} M HF+1×10^{-4} M $PdAc_2$ for different periods of time: (a) 30 s and (b, c) 5 min, respectively.

The attachment of the copper covering on the Si NW core is durable, as shown in Figure 4b. It is difficult to peel the copper covering from the Si NW core even with the help of sonication. Perhaps the dense copper covering (Figure 4b (inset)) prevents HF from permeating into the interior and hence dissolving the interfacial layer ("glue layer") between the copper and the Si NW. After being peeled off, flexible copper NWs are obtained, as shown in Figure 4c. Such an approach provides another possible route to fabricate a metal NW of 100 μm in length and 50−100 nm in diameter that is made of the self-assembled NPs and exhibits a semitubular shaped cross-sectional area (Figure 4b (inset)).

In Figure 4d (inset), the TEM picture illustrates the homogeneous growth of the individual NPs. It is in agreement with the phenomenon observed in Figure 2, suggesting that the aggregation dominates the growth process.[16−18] It is also found that the individual NPs are single crystals and there may be mismatch interconnection between two neighboring nanocrystals (Figure 4d).[41,42] In Figure 4e, the EDX spectrum confirms the formation of a relatively pure copper covering on the Si NW surface.

In the case of palladium, a totally different morphology is observed, as demonstrated in Figure 5. The palladium particles were not limited to the Si NW surface to form a metal covering but grew into the deposition solution to form a network, implying a fast growth process and a suppressed renucleation process on the Si NW surface.[31,44] A similar structure of palladium has been obtained when an alternating current (AC) electric field was used as the

(43) Föll, H.; Christophersen, M.; Carstensen, J.; Hasse, G. *Mater. Sci. Eng., R* **2002**, *39*, 93–141.

(44) Sun, X.-H.; Wong, N.-B.; Li, C.-P.; Lee, S.-T.; Kim, P.-S. G.; Sham, T.-K. *Chem. Mater.* **2004**, *16*, 1143–1152.

driving force for the deposition reaction.[45] In the present electroless redox reaction, the growth is random, whereas in the AC situation, a preferred growth direction is induced. In contrast to the Ag nanosticks and dendrites in images a and b in Figure 3, the fluffy palladium network in Figure 5 is primarily due to the attachment of the nanocrystals in a nonpreferential manner.[16−18] This kind of metallized NW could potentially lead to new and novel nanocomposite materials of importance in nanotechnology,[44] such as catalysts for organic and inorganic reactions.[11]

3.4. SERS Response from the Ag NPs Self-Assembled along the Si NW. It is well-known that an Ag NP array can be used as a SERS substrate.[19−21] To prepare a SERS substrate with a high enhancement and a uniform distribution, the metallization condition should be optimized, as shown in Figure 2 and Figures S1 and S2 in the Supporting Information. In Figure 6a, the deposition time was varied whereas the deposition solution was kept the same as the optimized one used in Figure 2. The highest intensity of Raman signal was collected from the Ag NP substrate with a deposition time of ~5 min, which corresponds to the structure presented in Figures 2f, g. Other Ag NP arrays with longer or shorter deposition time led to a decreased intensity. A possible reason is that the large particles or a bulk Ag covering has been produced after long deposition time (Figures S1c, d), which can decline the Raman enhancement.[30] Also, a short deposition time corresponds to a low density of NPs (Figures 2a−d), which again yields a weak Raman signal. Under the optimized deposition condition, a limit of detection of ~1 nM R6G was reached when incubation in the sample solution was employed to load the Raman scatterer (Figure 6b). Although a few assumptions are involved, and the optical arrangement of focusing on the NW is not optimal, the average enhancement factor of $\sim 1 \times 10^7$ is estimated for the experiments. This implies a pronounced SERS effect from this type of nanocomposite surface.

When the laser was focused on the metallized NW array to excite the Raman scattering, different intensities of the Raman scattering (Figure 6c) were observed from different positions (Figure 2g). The signal was significantly enhanced when the laser was focused on the Ag NPs assembled along the Si NW, as shown in Figure 6c ("wire" curve), whereas a weak signal or no signal was measured from the gap area between NWs.[8,30] One reason for this observation is that the deposition reaction was selective for the Si NW surface and not for the thick Si oxide layer in the gap area. Also, it should be mentioned that the diameter of a laser spot is ca. 1.0−1.5 μm and the interdistance between two neighboring NWs is 2 μm.[33] Therefore, a laser spot can not cover two NWs at one time. In other words, every Raman spectrum in this report was collected from a single metallized NW alone (or the gap),

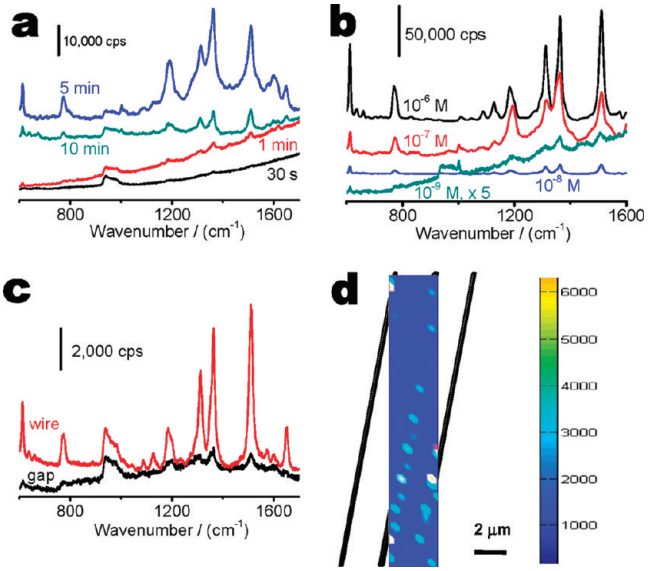

Figure 6. SERS intensity depending on (a) metallization time, (b) R6G concentration, (c) laser spot position, and (d) its mapping image from the Raman intensity at the peak of 1510 cm^{-1}. The metallization condition is presented in Figure 2 and the different deposition time is listed in (a) or just fixed for 5 min (b−d). The Raman scatterer's loading in (c, d) is different from that in (a, b), as discussed in the text. The different laser spot's position for (c) is indicated in Figure 2g. For clarity of presentation, NWs (gray strips) and the intensity scale are also presented in (d).

suggesting that the efficient enhancement arises from the assembled NPs.

The spectral intensity of the peak at 1510 cm^{-1} was selected to map the NW array. The corresponding results are presented in Figure 6d. From the intensity image, the NW's position is clearly identifiable against the blue background. This result supports the assumption that the strong Raman response comes from the Ag NPs self-assembled on a single NW alone.[8,47] The blue background indicates that there is little or no Raman response from the gap area (Figure 6c). Perhaps there are some residual Ag NPs in the gap area (Figures S1b, d in the Supporting Information), which contributes to the collected weak Raman signal. On the other hand, the Raman signal collected along the NW is much stronger than that from the gap area, from green to yellow spots, the intensity of which is uniform because of the close intensity of Raman signal (ca. 5000 cps)). The discrete nature of the high intensity signals along the NW is due to the 1 μm sampling intervals used in the mapping. Again, this suggests that regular arrays of NW can result in a uniform metal deposition and hence a uniform SERS activity.

In Figure 6c, a drop (~0.2 μL) of R6G solution of 1×10^{-7} M was spread onto a freshly metallized NW array. After drying in air, the Raman signal was promptly collected to test the possibility to prepare a fresh SERS substrate at the point of use. Assuming that all R6G molecules have been uniformly adsorbed onto the whole NW array area (~0.2 cm^2), there would be ~600 R6G molecules within a laser spot. In Figure 2f, there are at most 200−300 Ag NPs along one metallized NW within

(45) Cheng, C. D.; Gonela, R. K.; Gu, Q.; Haynie, D. T. *Nano Lett.* **2005**, *5*, 175–178.
(46) Doering, W. E.; Nie, S. *J. Phys. Chem. B* **2002**, *106*, 311–317.
(47) Song, W.; Li, W.; Cheng, Y.; Jia, H.; Zhao, G.; Zhou, Y.; Yang, B.; Xu, W.; Tian, W.; Zhao, B. *J. Raman Spectrosc.* **2006**, *37*, 755–761.

the size of a laser spot, indicating the high enhancement once again.[23,46] This situation is not far from single molecule detection.[23,48] That is because only the molecules that have been adsorbed onto the appropriate position, which is called as hot-spot, can yield the extremely enhanced Raman scattering and dominate the collected SERS signal.[20,46] Therefore, the above results confirm the existence of SERS hot-spots.[49−53] Although laser polarization should have an effect on the SERS signal collected from the hot-spot, this aspect has not been investigated, in part because of the ill-defined nature and orientations of the NW/NPs interfaces (i.e., images b and d in Figure 4).[52,54]

The high SERS enhancement means there is a strong electromagnetic field, which principally originates from the overlapping surface plasmon from the neighboring Ag NPs when they are located closely.[20] The small size of the Si NW provides a high specific surface area with a high degree of curvature for the Ag NP to nucleate and grow, which results in NPs with a characteristic size and morphology that is considerably different from that normally formed on a flat surface (Figure 2d). As a consequence, a close packing and unusual arrangement of Ag NPs can be achieved. The Ag NPs self-assemble along the Si NW template with a close interdistance, as shown in Figure 1b and Figure 2f.[9,55] In addition to the close interdistance, there is perhaps a higher density of hot-spots and each hot-spot probably have a larger volume.[56] Therefore, more molecules can be loaded into the hot-spot area and a stronger Raman response is in turn obtained. On the other hand, a contribution from chemical enhancement should not be ignored, because halide ions (Cl^-) are always present because of the sample preparation process.[46]

4. Conclusions

By combining nanotechnology with solutions of HF and metal ions,[27] a simple method was developed to metallize the Si NW. Not only Ag^+ but also Cu^{2+}, Pd^{2+}, Co^{2+}, Au^{3+}, and Pt^{4+} were reduced and deposited onto the NW surface. In some cases, further self-assembly into the metal covering or network was observed. Several new nanocomposite materials have been accordingly fabricated, such as metal NW with a semitubular shaped cross-section made of the self-assembled NPs, an Ag micrometerecklace, a palladium micrometeretwork and so on. Compared with the lithography patterned method to fabricate the metal NW, this one is seemingly facile.[57]

Of the above-mentioned nanocomposite materials, the Ag NP covered Si NW was used as a SERS substrate with a significant Raman enhancement. The regular arrangement of the NW array yielded a uniform SERS substrate by self-assembling the Ag NPs along the Si NW. It offers the possibility to prepare a fresh SERS substrate at the point of use that is oxide-free. The simple deposition procedure helps to avoid possible contamination from the storage or from the introduction of other reactant, such as reducing agent, surfactant, thioagent and so on.

Experiments also showed that a strong SERS signal could be collected from only one metallized NW. The detection of a small number of molecules from the self-assembled Ag NPs suggests strong SERS enhancement.[22] This approach holds promise for trace-level and perhaps single molecule detection.[48]

The present approach develops a simplified metallization platform and a facile method for the preparation of nanocomposite materials. It also brings new insights into the associated metal deposition process, various aspects of the SERS effect and the optical properties of these interesting nanocomposite materials.

Acknowledgment. The authors are grateful for the financial support of A*STAR, Singapore.

Supporting Information Available: More SEM pictures and detailed discussion on the metallization process of the Si NW (PDF). This material is available free of charge via the Internet at http://pubs.acs.org.

(48) Sawai, Y.; Takimoto, B.; Nabika, H.; Ajito, K.; Murakoshi, K. *J. Am. Chem. Soc.* **2007**, *129*, 1658–1662.
(49) Xu, H.; Bjerneld, E. J.; Käll, M.; Börjesson, L. *Phys. Rev. Lett.* **1999**, *83*, 4357–4360.
(50) Xu, H.; Aizpurua, J.; Käll, M.; Apell, P. *Phys. Rev. E* **2000**, *62*, 4318–4324.
(51) Gunnarsson, L.; Bjerneld, E. J.; Xu, H.; Petronis, S.; Kasemo, B.; Käll, M. *Appl. Phys. Lett.* **2001**, *78*, 802–704.
(52) Xu, H.; Käll, M. *Chemphyschem* **2003**, *4*, 1001–1005.
(53) Xu, H.; Käll, M. *Top. Appl. Phys.* **2006**, *103*, 87.
(54) Yoon, I.; Kang, T.; Choi, W.; Kim, J.; Yoo, Y.; Joo, S.-W.; Park, Q.-H.; Ihee, H.; Kim, B. *J. Am. Chem. Soc.* **2008**, *131*, 758–762.
(55) Becker, M.; Sivakov, V.; Andra, G.; Geiger, R.; Schreiber, J.; Hoffmann, S.; Michler, J.; Milenin, A. P.; Werner, P.; Christiansen, S. H. *Nano Lett.* **2007**, *7*, 75–80.
(56) Le, F.; Brandl, D. W.; Urzhumov, Y. A.; Wang, H.; Kundu, J.; Halas, N. J.; Aizpurua, J.; Nordlander, P. *ACS Nano* **2008**, *2*, 707–718.
(57) Xiang, C.; Kung, S. -C.; Taggart, D. K.; Yang, F.; Thompson, M. A.; Guell, A. G.; Yang, Y.; Penner, R. M. *ACS Nano* **2008**, *2*, 1939–1949.